Communications: SIF Congress 2010

Magnetization dynamics in thin magnetic films with spatio-temporal resolution

Ch. Piovera

CNR-IFN, Ultras, Dipartimento di Fisica, Politecnico di Milano
Piazza Leonardo da Vinci 32, 20133 Milano, Italy

Summary. — Based on the Magneto-Optical Kerr Effect (MOKE), we have fully characterized the magnetization dynamics in thin magnetic films by measuring the three real-space components of the magnetization vector. Using the pump-probe technique it is possible to extract the time dependence of each individual projection with sub-picosecond resolution. This method has been exploited to investigate the temporal evolution of the magnetization (modulus and orientation) induced by an ultrashort laser pulse in thin epitaxial iron films. According to our results, we deduced that the initial sub-picosecond demagnetization is established at the electronic level through electron-magnon excitations. The subsequent dynamics is characterized by a precessional motion on the sub-nanosecond time scale, around an effective, time-dependent field. The temporal evolution of the magneto-crystalline anisotropy constant can be unambiguously determined, providing the experimental evidence that the precession is triggered by the rapid, optically induced misalignment between the magnetization vector and the effective field. These results suggest a possible pathway toward the ultrarapid switching of the magnetization.

PACS 75.70.-i – Magnetic properties of thin films, surfaces, and interfaces.
PACS 78.20.Ls – Magneto-optical effects.
PACS 75.30.Ds – Spin waves.
PACS 78.47.-p – Spectroscopy of solid state dynamics.

1. – Introduction

Disclosing the elementary excitations in ferromagnets, and in particular the processes governing spin dynamics on the femtosecond time scale, is one of the most challenging subjects in modern solid-state physics. As a matter of fact, despite the considerable experimental evidence gathered in the last decade, microscopic models of the ultrafast spin behavior have been proposed only recently [1-4], and they are still under debate. On the other hand, its understanding could be the keystone for novel applications in spintronics and one of the possible paths towards the speed enhancement of magnetic

recording devices. In this scenario, femtosecond laser pulses offer the intriguing possibility to probe a magnetic system on a time scale faster or comparable with fundamental spin interactions: 10–100 fs for exchange interactions, 0.1–1 ps for spin-orbit coupling and about 100–1000 ps for magnetic precessions. It is well established, nowadays, that the excitation of a ferromagnet through an ultrashort laser pulse induces a demagnetization in the sub-picosecond regime and we can disclose the ultrafast interaction mechanisms by measuring such a rapid modification. When photons, focused on a metal, are absorbed by electrons close to the Fermi level, they originate a nonequilibrium distribution that thermalizes with the surrounding environment (other electrons and lattice) via electron-electron and electron-phonon scattering [5-9]. In ferromagnetic materials the spin order is an additional factor that must be considered. Scattering events can induce spin-flips through different mechanisms such as Stoner excitations, electron-magnon interaction and phonon-mediated spin-flips (also known as Elliot-Yafet events), affecting the net magnetization of the sample (less than 100 fs).

On a larger time scale (sub-nanoseconds), it has been shown that spin order can be manipulated through precessional dynamics. A free magnetic moment misaligned with respect to a magnetic field undergoes a gyroscopic motion (known as Larmor precession) caused by the torque the field exerts on it. In particular, in our case, laser pulses act as heat source and affect the magnetic anisotropy that forces spins to converge towards preferential directions (the easy axes). When the local thermal equilibrium among electrons has been achieved (less than 1 ps), the temperature rises to several hundred kelvin and a step change in anisotropy takes place triggering the magnetization precession [10-12]. The period of that motion depends on the intensity of the field and lies in the picosecond regime for intensities of the order of a tesla. That time scale attracts technological interest on ferromagnetic materials, since the precession mechanism provides a way to switch the magnetization between different states [13]. In fact in standard quasi-static conditions (*i.e.* for slowly varying external magnetic fields), the magnetization moves between easy axes through slow processes such as magnetic domain nucleation and domain wall motion [14] (the domain wall velocity is 10^3–10^4 ms in Fe films [15]).

In the following we present a time-resolved MOKE (Magneto-Optical Kerr Effect) experimental configuration capable to retrieve quantitative sub-picosecond information about magnetization in thin epitaxial Fe(001)/MgO(001). The magneto-optical Kerr effect can be fully understood in terms of Fresnel scattering matrix formalism: it is essentially based on the variation of the light polarization state reflected from a magnetic surface [16]. In particular, we managed to measure the complete magnetization vector (*i.e.* the real-space 3D components) by performing two different measurements and exploiting simple symmetry relations [17]. We note already here that all the data have been acquired without modifying either the sample position or the detection geometry. In this way we show that the magnetization undergoes a precessional motion triggered by the rapid change of the magneto-crystalline anisotropy after an intense infrared laser pulse. Our approach allows us to determine the heat-induced dynamics of the anisotropy field and provides the direct experimental evidence of the mechanism that launches the precession.

2. – Experimental details

The thin Fe(001) films (about 8 nm thick) were epitaxially grown on MgO(001) single crystalline substrates. Prior to the deposition, the substrates were cleaned by repeated cycles of sputtering with 1 kV Ar^+ ions and annealing up to 800 K in ultra-high vacuum (base pressure of 10^{-10} mbar). The Fe deposition was performed with an electron-beam
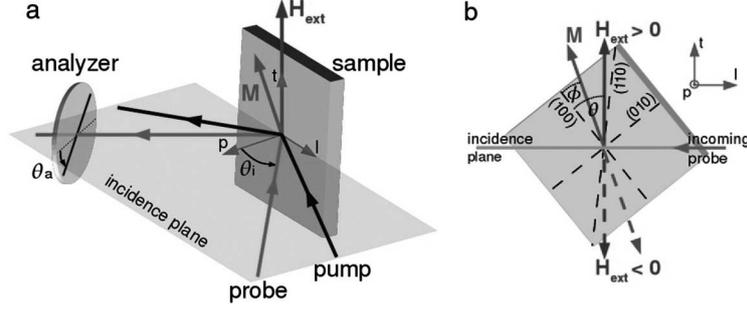
Fig. 1. – (a) Experimental geometry: the p-polarized pump and probe beams lie on the same incidence plane. The external magnetic field $\mathbf{H}_{ext}$ is applied along the sample surface and normal to the incidence plane. (b) External field $\mathbf{H}_{ext}$ and magnetization $\mathbf{M}$ form the angles θ and ϕ, respectively, with the [100] easy axis of the epitaxial Fe(001) film.

evaporator at a rate of about $0.2\,\mathrm{nm/min}$ to the substrates held at room temperature. After the deposition, the samples were annealed to about $750\,\mathrm{K}$, in order to reduce the possible defects formed during the epitaxial growth, and characterized through Low Energy Electron Diffraction (LEED). The optical analysis has been performed *ex situ* with an amplified Ti:Sapphire laser, generating $50\,\mathrm{fs}$ pulses centered at $800\,\mathrm{nm}$ ($1.55\,\mathrm{eV}$) with a repetition rate of $1\,\mathrm{kHz}$. For dynamics investigations, the time-resolution has been achieved via the pump-probe technique with the pump beam focused to a spot size of about $200\,\mu\mathrm{m}$ and an average fluence of a few $\mathrm{mJ/cm^2}$. The MOKE analysis has been performed with p-polarized probing beam hitting the sample at an incident angle $\theta_i \sim 45°$ with respect to the surface normal (see fig. 1a). The probe beam reflected from the sample passed through an analyzer (Glan-Thompson polarizer) oriented at an angle θ_a from the plane of incidence and was then detected by a photodiode. Before hitting the sample, a small portion of the probe beam illuminated a second photodiode identical to the first one and the electrical signals from the two detectors were fed into the differential input of a lock-in amplifier. The beam intensities on the two diodes were adjusted in order to obtain coincident photocurrents, allowing us to operate at high sensitivity and at the laser frequency of $1\,\mathrm{kHz}$, without further beam modulation [18]. The external magnetic field $\mathbf{H}_{ext}$ was produced by two Helmholtz coils and was applied normal to the incidence plane (thus parallel to the sample surface).

2˙1. *The magnetization vector*. – Referring to fig. 1a, the magnetization vector $\mathbf{M}$ can be decomposed into projections named according to their orientation relative to the plane of incidence: the transverse and the longitudinal components, M_t and M_l, lie along the Fe film and are perpendicular and parallel to the incidence plane, respectively (thus, $M_t \parallel \mathbf{H}_{ext}$), while the polar component M_p is normal to the sample surface. Within this frame of reference, using the Fresnel scattering matrix formalism, the beam intensity I after the analyzer and normalized to the incident intensity, can be written as [19]:

$$(1) \qquad I(\theta_a) = (A + Bm_t)\cos^2\theta_a + (Cm_l + Dm_p)\cos\theta_a \sin\theta_a,$$

where A, B, C and D are real coefficients depending on the complex refractive index, the magneto-optical constant of the material and the incidence angle θ_i, while $m_t = M_t/M_s$, $m_l = M_l/M_s$ and $m_p = M_p/M_s$, with M_s the saturation magnetization. The
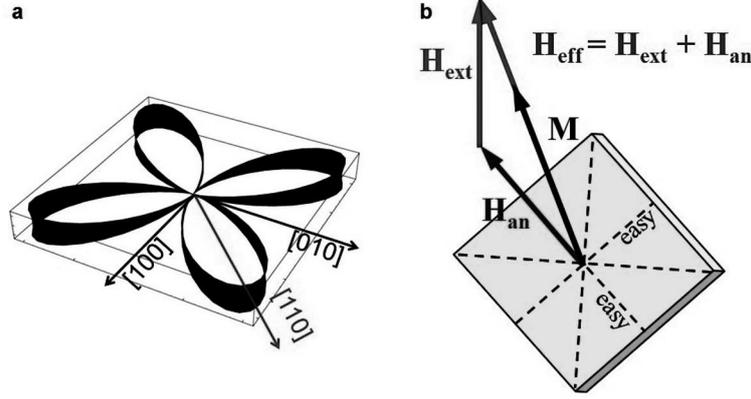
Fig. 2. – (a) In a pictoresque view, the black line represents the four minima of the free-energy density as a function of the magnetization direction in the real space: [100] and [010] are the easy axes separated by energy barriers (the hard axes). (b) For small angle ϕ the magnetization vector aligns with the vectorial sum of the anisotropy and external field.

θ_a dependence of the beam intensity in eq. (1) suggests a way to separate the different components: by measuring I at two opposite orientation of the analyzer, it is easily shown that (for $\theta_a = 45°$):

$$(2) \qquad\qquad I_{sum} = I(\theta_a) + I(-\theta_a) = A + Bm_t,$$
$$(3) \qquad\qquad I_{diff} = I(\theta_a) - I(-\theta_a) = Cm_l + Dm_p.$$

These relationships permit a first separation of the magnetization projections. Moreover, the coefficients C and D have opposite parities with respect to the incidence angle (they are an even and an odd function of θ_i respectively). This allows one to fully distinguish the three vectorial components m_t, m_l and m_p:

$$(4) \qquad\qquad I_{diff}(+\theta_a) - I_{diff}(-\theta_a) = 2Cm_l,$$
$$(5) \qquad\qquad I_{diff}(+\theta_a) + I_{diff}(-\theta_a) = 2Cm_p.$$

These relations represent the backbones to quantitatively determine the real-space components of the magnetization vector and they will be exploited in the following sections.

2˙2. *Fe thin film: the magnetic anisotropy.* – The as-grown magnetic Fe layer is characterized by a biaxial in-plane and a strong shape anisotropy. Therefore, without any applied field the magnetization $\mathbf{M}$ lies on two preferential directions of the surface plane and there is no polar component (*i.e.* $m_p = 0$). For our thin film these crystallographic directions are the (100) and the (010) as shown in fig. 2a where the black fourfold line represents, in a pictoresque view, the four easy axes corresponding to four energetic minima. In fact the magnetic anisotropy can be described by the free-energy density g which is a function of the direction of the $\mathbf{M}$ vector in real space. For a planar biaxial system we have (in dimensionless form):

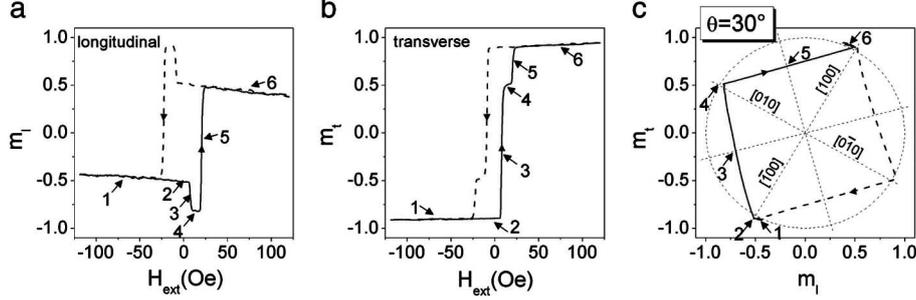$$(6) \qquad\qquad g = \frac{1}{8}\sin^2 2\phi - \frac{H_{ext}}{H_{an}}\cos(\phi - \theta),$$

Fig. 3. – Normalized longitudinal (a) and transverse (b) projections of the hysteresis loop for the external field applied at $\theta = 30°$ from the (100) easy axis. (c) 2D graph of the transverse *vs.* longitudinal projections depicting the trajectory of the magnetization vector on the film plane. In all three graphs, the numbered arrows help relate the different positions of the trajectory with the corresponding points on the hysteresis loops.

where ϕ (respectively θ) is the angle on the film plane formed by the magnetization vector $\mathbf{M}$ (the external field $\mathbf{H}_{ext}$) with the (100) axis (see fig. 1b). $\mathbf{H}_{an}$ is the intensity of the so-called anisotropy field lying along the easy axes and equal to $\mathbf{H}_{an} = 2K_1/\mu_0 M_s$, where K_1 is the magneto-crystalline anisotropy constant. The value of $\mathbf{H}_{an}$ amounts to about 550 Oe for bulk iron. It can be shown that for a small angle ϕ, the quantity g is equivalent to the energy term $-\mu_0 \mathbf{M} \cdot (\mathbf{H}_{ext} + \mathbf{H}_{an})$. This means that in the presence of an external field, the magnetization vector aligns with the effective field given by the sum $\mathbf{H}_{eff} = \mathbf{H}_{ext} + \mathbf{H}_{an}$ as shown in fig. 2b. In conclusion we can say that the free energy g has several local minima, representing the angular equilibrium positions of the magnetization, *i.e.* the easy axes, which are separated by energy barriers determined by the magneto-crystalline anisotropies. If the modulus of the applied field $\mathbf{H}_{ext}$ or its orientation θ change, the local minima of g shift, leading to the coherent rotation of $\mathbf{M}$. However, the transition from one local minimum to another one can take place via domain wall motion rather than coherent rotation reversal as we will discuss in the following sections.

We will first restrict our analysis to the quasi-static characterization of the in-plane magnetization (m_l and m_t) and the reversal processes under the effect of the external field. Then, we will extend our investigation to the dynamic case (pump-probe experiments).

3. – Quasi-static case: in-plane magnetization ($m_p = 0$)

In quasi-static conditions with the applied field lying on the film plane, the polar component is absent because of the strong shape anisotropy. Therefore with $m_p = 0$ and $\mathbf{H}_{ext}$ spanning from $+40$ Oe to -40 Oe, it is easy to see that we can measure the hysteresis loops of $m_l(\mathbf{H}_{ext})$ and $m_t(\mathbf{H}_{ext})$ exploiting eqs. (2) and (3). Figures 3a and b show an example of the projections of the two hysteresis loops acquired with an orientation $\theta = 30°$ of the sample. At this point if one plots the transverse component m_t as a function of the longitudinal one, m_l, as reported in fig. 3c, the in-plane path of the magnetization vector is disclosed and the specific mechanism of magnetization motion can now be explained. The small arrows (in fig. 3) help relating the positions on the $m_l(\mathbf{H}_{ext})$ and $m_t(\mathbf{H}_{ext})$ loops to the corresponding points along the two-dimensional

trajectory. Now, focusing on the branch corresponding to the increasing applied field (from negative to positive values, solid lines) interesting features come out:

1. For high external fields (arrows 1 and 6) the magnetization is saturated (its modulus is M_s). The sample is in the single magnetic domain state and under the effect of the field the magnetization vector changes direction keeping its modulus constant. This behavior represents the well-known coherent rotation regime [20] in which the trajectory is tangent to the dashed circle of unitary radius in fig. 3c.

2. At remanence ($\mathbf{H}_{ext} = 0$, arrow 2) the magnetization vector is aligned to the $[\bar{1}00]$ easy axis.

3. The steep changes marked by arrows 3 and 5 correspond to the magnetization switching between easy axes. Increasing the applied field from negative to positive values, the magnetization moves from the $[\bar{1}00]$ to the $[010]$ direction (arrow 4) and then to the $[100]$ axis with two separate steps. These transitions are characterized by straight paths (fig. 2c) where the modulus of the magnetization is clearly not conserved. In fact during both switching processes, magnetic domains start to nucleate along the new axis, and then grow through domain wall motion. The magnetic vector is described by its projections along the easy axes, for example $M_{[010]}$ and $M_{[100]}$ for the switch marked by arrow 5. In order to conserve the total microscopic magnetic moments, the relation $M_{[100]} + M_{[010]} = M_s$ must be satisfied. This is exactly the analytical form of the linear path experimentally observed.

4. – Ultrafast demagnetization

In this section we will show how a short and intense laser pulse modifies the previously highlighted magnetization trajectories. The time-resolution is achieved with the pump-probe method: the hysteresis loops are now measured setting a fixed delay between the probing beam and the intense pump pulses. By varying this delay, we can measure the dynamics of the magnetization vector and, in particular, the effects induced by the impulsive excitation. The temporal resolution of these experiments is determined by the laser pulse duration and is of the order of 50 fs. Figure 4a reports the two-dimensional trajectories of the in-plane magnetization as a function of the pump-probe delay (vertical axis) for the external field orientation $\theta = 30°$. It can be immediately seen how the optical pumping leads to a rapid and rather uniform demagnetization, *i.e.* reduction of the M_s modulus with very similar in-plane trajectories, in agreement with the previous measurements on thin Fe films [21]. This effect is clearly evidenced in fig. 4b, showing the magnetization path recorded for negative pump-probe delay (*i.e.* the probe precedes the pump) and 500 fs after the pump. Moreover, with regard to the switching process between easy axes, we can say that the previously illustrated mechanism is not affected by the optical pumping. Figure 4c reports the temporal evolution of M_s measured at remanence along the [100] easy axis. The demagnetization takes place within 100 fs past the pump pulse perturbation, while the subsequent recovery seems to involve two well-discernible processes with different time constant: a fast one (a few ps) and a slow one (several tens of ps). The latter is attributed to heat diffusion outside the irradiated area, the former is related to phonon-mediated relaxation processes.

In particular, as already shown in [18], laser-induced ultrafast demagnetization of epitaxial Fe thin films can be understood in terms of electron-magnon interaction, taking place on a time scale < 100 fs. Hot electrons can efficiently excite magnons, leading
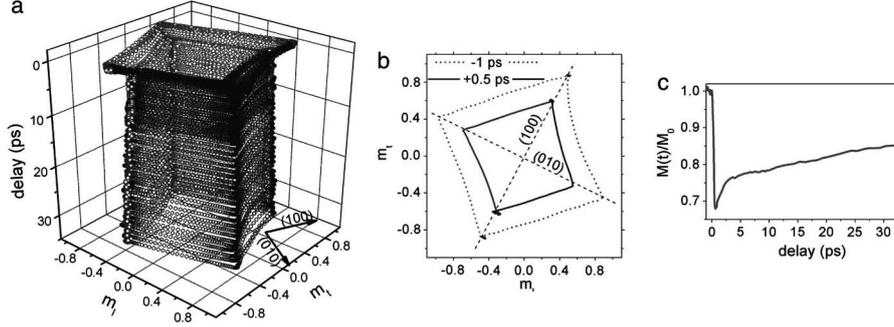
Fig. 4. – (a) Temporal evolution of the in-plane magnetization trajectories induced by the pump pulse for $\mathbf{H}_{ext}$ at about $\theta = 30°$ from the easy axis. (b) In-plane magnetization trajectories 1 ps before (dashed line) and 0.5 ps after (solid line) the effect of the pump pulse. (c) Temporal evolution of the normalized magnetization at remanence (along the easy axis).

to a rapid reduction in the magnetization. This process is mediated by the spin-orbit coupling, allowing the transfer from spin to orbital angular momentum that is eventually absorbed by the lattice. The subsequent recovery of the spin order takes place with a characteristic time constant of ~ 800 fs, that is longer than the electron-phonon relaxation time of 240 fs, and supports the picture of Elliot-Yafet spin-flip scattering. That interpretation represents an alternative explanation of the ultrafast demgnetization mechanism, as compared to other existing models [22].

5. – Precession dynamics

In the previous section we described the behavior of the magnetization in the first few picoseconds after the short and intense laser pulse perturbation. However, under specific experimental conditions, we have measured a longer dynamics that lasts hundreds of picoseconds. As already demonstrated in some experiments [12,23,24], the $\mathbf{M}$ vector undergoes a precessional motion when it experiences a rapid misalignment with respect to the effective magnetic field $\mathbf{H}_{eff}$. When the involved fields are of the order of a tesla, this precession has a period lying in the picosecond regime. In our case the magnetization is parallel to the vectorial sum $\mathbf{H}_{an} + \mathbf{H}_{ext}$ (not aligned with an easy axis, see fig. 2b), thus only a rapid change of the crystalline anisotropy can induce a Larmor gyroscopic motion around $\mathbf{H}_{eff}$. In particular with the help of numerical simulations [12, 23], it has been shown that a prompt decrease of the magneto-crystalline anisotropy happens because of laser heating. Therefore we have developed an experimental configuration that, compared to the mentioned one [24], allows us to quantitatively retrieve the dynamics of the magneto-crystalline anisotropy. A precessional motion induces a periodic out-of-plane (polar) component of the magnetization that must be isolated from the in-plane ones. Referring to eqs. (4) and (5) we already know that m_l and m_p can be determined by measuring the MOKE signal for opposite incidence angle of the probe beam. However, according to symmetry considerations (fig. 1b) it can be seen that inverting θ_i is equivalent to inverting the applied magnetic field. In this way all the three spatial projections of the magnetization vector can be unequivocally separated without any modification of the experimental setup but just changing the analyzer angle and the direction of the external field.
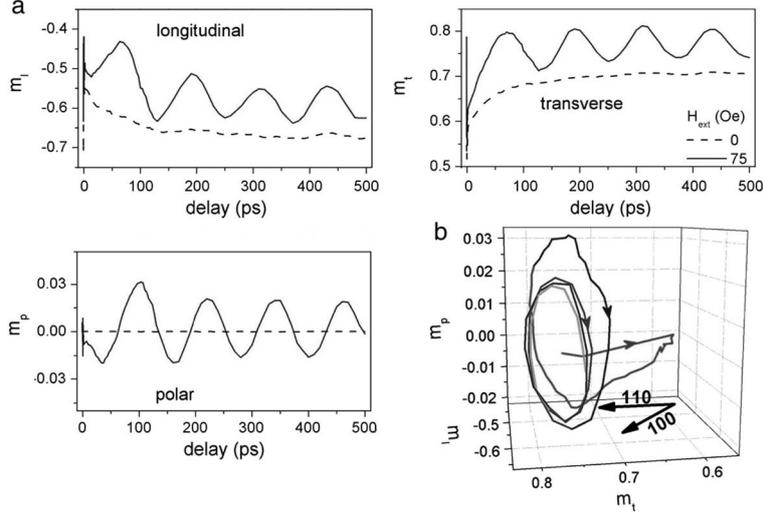
Fig. 5. – (a) Longitudinal, transverse and polar (top to bottom) components of the magnetization vector *vs.* pump-probe delay, for two values of the external field (0 and 75 Oe). The angle between $\mathbf{H}_{ext}$ and the (100) easy axis is $\theta = 44°$. (b) 3D view of the real-space trajectory of the vector $\mathbf{M}$ (for $\mathbf{H}_{ext} = 75$ Oe).

Figure 5 reports the m_t, m_l and m_p components measured for an angle $\theta = 44°$ (*i.e.* the applied field was almost collinear to the (110) hard axis) in order to maximize the gyroscopic effect. Without external field, no oscillation and no polar component are present (dashed lines). The modulus of the magnetization vector rapidly drops by about 30% at 0 ps delay and then slowly recovers within a few hundreds of picoseconds. In the presence of the external field (solid lines), the oscillatory behavior becomes clearly visible, with a period of roughly 120 ps. The 3D trajectory of the magnetization is reconstructed in fig. 5b. After the initial drop of the magnetization, the subsequent recovery is characterized by a well-discernible gyroscopic motion. The amplitude of the coils reduces, while their center shifts toward the (100) crystallographic direction as the system relaxes toward equilibrium. This motion is usually described by the well-known Landau-Lifshitz-Gilbert (LLG) equation [25], according to which the vector $\mathbf{M}$ precesses around the effective field and experiences a dissipative damping that hampers the oscillations. Eventually, the magnetization will align along $\mathbf{H}_{eff}$, that represents the axis of the precessional cone. Thus the effective field is time dependent and moves in the film plane. When the local thermal equilibrium is established (within a picosecond), both saturation magnetization $\mathbf{M}_s$ and magneto-crystalline anisotropy constant $\mathbf{K}_1$ assume their quasi-static temperature dependence. In particular, for high temperature the intensity of the anisotropy field $\mathbf{H}_{an} \sim K_1/M_s$ drops. According to our geometry (see fig. 2b), the total effective field decreases and rotates towards $\mathbf{H}_{ext}$ inducing the precession, while after the heat dissipation away from the irradiated area, it comes back to its initial value.

At this point, exploiting some easy trigonometrical tricks, it easy to see that the modulus and orientation of $\mathbf{H}_{an}$ can be retrieved from the magnetization trajectory. In fact when the polar component is maximum, the projection of $\mathbf{M}$ on the film plane is parallel to the precessional axis which is, in turn, the sum of the $\mathbf{H}_{ext}$ (experimentally fixed) and $\mathbf{H}_{an}$. Now, with the help of eq. (6), knowing ϕ we can deduce $\mathbf{H}_{an}$ as a function of the
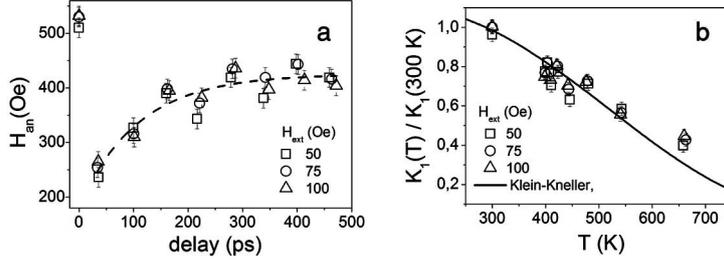
Fig. 6. – (a) Experimental evolution of the (in-plane) magneto-crystalline anisotropy field *vs.* pump-probe delay (the dashed line is a guide for the eye). (b) Temperature dependence of the magneto-crystalline anisotropy constant for three external magnetic fields (symbols), normalized to its room temperature value, as obtained from the data. The solid line is taken from ref. [27], for comparison.

pump-probe delay. Figure 6a reports the temporal evolution of the magneto-crystalline anisotropy field obtained independently from three sets of data corresponding to the applied fields $\mathbf{H}_{ext}$ of 50, 75 and 100 Oe. At a negative delay (slightly before the pump hits the sample) the extrapolated value of $\mathbf{H}_{an}$ compares well with the anisotropy field of bulk iron (550 Oe), but, after pumping, it drops to about half of its initial value, and slowly recovers within a few hundreds of ps. Since $\mathbf{H}_{an} \sim K_1/M_s$, the time evolution of the magneto-crystalline anisotropy constant K_1 can be readily deduced. Furthermore, the temporal abscissa of fig. 6a can be converted into a temperature scale [26] and the magneto-crystalline anisotropy constant K_1 evinced from our measurements can be plotted as a function of the local temperature, as reported in fig. 6b. Our experimental results are compared with the known temperature dependence of K_1 [27]. The remarkable agreement strongly reinforces our interpretation of the mechanism triggering the precessional motion and endorses the reliability of the experimental method.

6. – Conclusions

Based on the Magneto-Optical Kerr Effect (MOKE), we have characterized the magnetization of thin epitaxial iron films in quasi-static and dynamic conditions. We have measured the magnetization trajectory as a function of an applied field elucidating the switching mechanisms between easy axes. By means of the pump-probe technique, it is also possible to investigate the magnetization dynamics induced by an impulsive optical excitation. In particular, the loss of spin order (demagnetization) triggered by electron-magnon scattering processes is observed on the sub-picosecond time scale while, on the sub-nanosecond regime and under specific experimental conditions, a precessional motion can be triggered by the rapid, optically-induced misalignment between the magnetization vector and the effective field.

* * *

REFERENCES

[1]   ZHANG G. P. and HÜBNER W., *Phys. Rev. Lett.*, **85** (2000) 3025.
[2]   ZHANG G. P., HÜBNER W., LEFKIDIS G., BAI Y. and GEORGE T. F., *Nat. Phys.*, **5** (2009) 499.
[3]   BIGOT J.-Y., VOMIR M. and BEAUREPAIRE E., *Nat. Phys.*, **5** (2009) 515.
[4]   KOOPMANS B., MALINOWSKI G., DALLA LONGA F., STEIAUF D., FÄHNLE M., ROTH T., CINCHETTI M. and AESCHLIMANN M., *Nat. Mater.*, **9** (2009) 259.
[5]   BEAUREPAIRE E., MERLE J.-C., DAUNOIS A. and BIGOT J.-Y., *Phys. Rev. Lett.*, **76** (1996) 4250.
[6]   KOOPMANS B., VAN KAMPEN M., KOHLHEPP J. T. and DE JONGE W. J. M., *Phys. Rev. Lett.*, **85** (2000) 844.
[7]   RHIE H.-S., DÜRR H. A. and EBERHARDT W., *Phys. Rev. Lett.*, **90** (2003) 247201.
[8]   LISOWSKI M., LOUKAKOS P. A., MELNIKOV A., RADU I., UNGUREANU L., WOLF M. and BOVENSIEPEN U., *Phys. Rev. Lett.*, **95** (2005) 137402.
[9]   CINCHETTI M., SANCHÉZ ALBANEDA M., HOFFMANN D., ROTH T., WÜSTENBERG J.-P., KRAUSS M., ANDREYEV O., SCHNEIDER H. C., BAUER M. and AESCHLIMANN M., *Phys. Rev. Lett.*, **97** (2006) 177201.
[10] VAN KAMPEN M., JOZSA C., KOHLHEPP J. T., LECLAIR P., LAGAE L., DE JONGE W. J. M. and KOOPMANS B., *Phys. Rev. Lett.*, **88** (2000) 227201.
[11] ZHANG QIANG, NURMIKKO A. V., ANGUELOUCH A., XIAO G. and GUPTA A., *Phys. Rev. Lett.*, **89** (2002) 177402.
[12] VOMIR M., ANDRADE L. H. F., GUIDONI L., BEAUREPAIRE E. and BIGOT J.-Y., *Phys. Rev. Lett.*, **94** (2005) 237601.
[13] BACK C. H., ALLENSPACH R., WEBER W., PARKIN S. S. P., WELLER D., GARWIN E. L. and SIEGMANN H. C., *Science*, **285** (1999) 864.
[14] BERTOTTI G., *Hysteresis in Magnetism* (Academic Press, San Diego, USA) 1998.
[15] RUIZ-FEAL I., MOORE T. A., LOPEZ-DIAZ L. and BLAND J. A. C., *Phys. Rev. B*, **65** (2002) 054409.
[16] YANG Z. J. and SCHEINFEIN M. R., *J. Appl. Phys.*, **74** (1993) 6810.
[17] CARPENE E., MANCINI E., DALLERA C., PUPPIN E. and DE SILVESTRI S., *J. Appl. Phys.*, **108** (2010) 063919.
[18] CARPENE E., MANCINI E., DALLERA C., BRENNA M., PUPPIN E. and DE SILVESTRI S., *Phys. Rev. B*, **78** (2008) 174422.
[19] CARPENE E., MANCINI E., DAZZI D., DALLERA C., PUPPIN E. and DE SILVESTRI S., *Phys. Rev. B*, **81** (2010) 060415.
[20] STONER E. C. and WOHLFARTH E. P., *Philos. Trans. R. Soc. London, Ser. A*, **240** (1948) 599.
[21] KAMPFRATH T., ULBRICH R. G., LEUENBERGER F., MÜNZENBERG M., SASS B. and FELSCH W., *Phys. Rev. B*, **65** (2002) 104429.
[22] KOOPMANS B., KICKEN H. H. J. E., VAN KAMPEN M. and DE JONGE W. J. M., *J. Magn. Magn. Mater.*, **286** (2005) 271.
[23] BIGOT J.-Y., VOMIR M., ANDRADE L. H. F. and BEAUREPAIRE E., *Chem. Phys.*, **318** (2005) 137.
[24] VOMIR M., ANDRADE L. H. F., BEAUREPAIRE E., ALBRECHT M. and BIGOT J.-Y., *J. Appl. Phys.*, **99** (2006) 08A501.
[25] GILBERT T. L., *IEEE Trans. Magn.*, **40** (2004) 3443.
[26] HANHAM S. D., ARROTT A. S. and HEINRICH B., *J. Appl. Phys.*, **52** (1981) 1941.
[27] KLEIN H.-P. and KNELLER E., *Phys. Rev.*, **144** (1966) 372.